VSP

Journal of Adhesion Science and Technology 22 (2008) 319–334

Journal of ADHESION SCIENCE and TECHNOLOGY
www.brill.nl/jast

Electrowetting on Superhydrophobic Surfaces: Present Status and Prospects

Jason Heikenfeld * **and Manjeet Dhindsa**

Novel Devices Laboratory, Department of Electrical Engineering, University of Cincinnati, Cincinnati, OH 45221, USA

Abstract

Electrowetting devices with an initial superhydrophobic water contact angle (>150°) have now been demonstrated on a variety of structured substrates. These substrates are more complex than a conventional superhydrophobic surface since electrowetting requires an electrical conductor that is coated with a high-performance dielectric and a hydrophobic fluoropolymer. Substrate structures that have been studied include silicon nanoposts and nanowires, carbon nanofibers and nanotubes, and polymer microposts. Even though these structured surfaces are geometrically diverse, there are several consistencies in electrowetting behavior for all these platforms. As an electrowetting bias of 10's of volts is applied between a saline drop and the substrate, the macroscopically observed contact angle is typically decreased from >150° to ∼100°. As the voltage is increased an electromechanical force promotes capillary wetting between the substrate structures, and the saline drop transitions from the Cassie state to the Wenzel state. The Wenzel state presents a new energy minimum for the system, and in all current experiments the wetting is irreversible. Transition from the Wenzel state back to the Cassie state has been demonstrated by means of liquid boiling or addition of a second non-polar liquid. The importance of these recent investigations includes the dynamic tuning of the wetting on a superhydrophobic surface, and improved understanding of electrowetting on, and into, structured surfaces.

© Koninklijke Brill NV, Leiden, 2008

Keywords

Electrowetting, superhydrophobic, nanostructures, nanofibers, nanotubes, wetting

1. Introduction

Although superhydrophobic surfaces are far from a new research topic, real-time dynamic tuning of their wetting properties has seen increased interest in recent years. These new investigations have been partially fueled by an explosion of interest in electrowetting research [1], a field that has seen ∼70% annual growth in patents and publications since 2001 [2]. Electrowetting involves application of electrical potential across a liquid/dielectric/electrode capacitor, a charge-induced imbalance of forces near the liquid/dielectric contact line, and a resulting decrease

* To whom correspondence should be addressed. Tel.: 513-556-4763; e-mail: heikenjc@email.uc.edu

© Koninklijke Brill NV, Leiden, 2008 DOI:10.1163/156856108X295347

in the observed liquid contact angle. Several electrowetting technologies are already well on their way to commercialization, including those used for liquid lenses [3, 4], lab-on-chip [5, 6], and electronic displays [7, 8]. Investigation of electrowetting on superhydrophobic surfaces has been a more recent research topic. For electrowetting contact angle on superhydrophobic surfaces, the thought of electrowetting from a superhydrophobic ($>150°$) to a superhydrophilic state is understandably enticing. However, the present reality is that the electrowetted contact angle change is much more limited. Reports do show consistent transitions from the Cassie to the Wenzel wetting state. Reports also show that even for complex nanostructured surfaces, electrowetting behavior parallels many features of conventional wetting of structured surfaces. Here, a review is provided of recent results in electrowetting on superhydrophobic surfaces. The fundamentals of electrowetting on planar and structured surfaces are first presented. Fabrication techniques for superhydrophobic electrowetting structures are reviewed. Electrowetting results are then discussed, including recent efforts in achieving wetting reversibility. Lastly, speculations on techniques for improved reversibility and non-silicon style fabrication are provided.

2. Electrowetting on Planar and Structured Surfaces

The most basic form of a modern electrowetting structure consists of a sessile droplet, planar fluoropolymer dielectric, a planar substrate, and a DC voltage source (Fig. 1a). Electrowetting can be performed without a physical dielectric but a non-insulated liquid/electrode system is not highly reversible and will not be reviewed here. Theoretical predictions of electrowetting behavior can be derived using energy minimization [9], interfacial thermodynamics [10], or electromechanics [11]. All three approaches can be utilized to predict the macroscopically observed change in contact angle. However, a recent study by Mugele and Buehrle [12] has confirmed that the electromechanical approach developed by Jones *et al.* [11] is the most correct approach when including the meniscus profile at the microscopic scale (i.e. near the contact line). For an electrowetted droplet Mugele and Buehrle provided supporting theory and direct observation that the contact angle remains unchanged near the contact line even as voltage is applied and the droplet is macroscopically observed to decrease in contact angle.

The diagram in Fig. 1a shows that the initial angle is always Young's, as determined by interfacial tensions (γ) at the three-phase saline (S), ambient (A), fluoropolymer (F) contact line. The ambient can be air ($\gamma_{SA} \sim 73$ mN/m) or hydrocarbon oil ($\gamma_{SA} < 50$ mN/m). Widely utilized fluoropolymers include solution-processed DuPont Teflon AF and Asahi Cytop, both with $\gamma_{FA} \sim 16$–20 mN/m. As voltage is applied to this system, the saline/dielectric/electrode capacitor is charged. These charges consist of self-ionized water, ionized salt content such as 0.1 M KCl, and/or in some cases, ionic surfactant content such as sodium dodecyl sulfate. It is the charge density near the contact line that results in electrical field with a partial

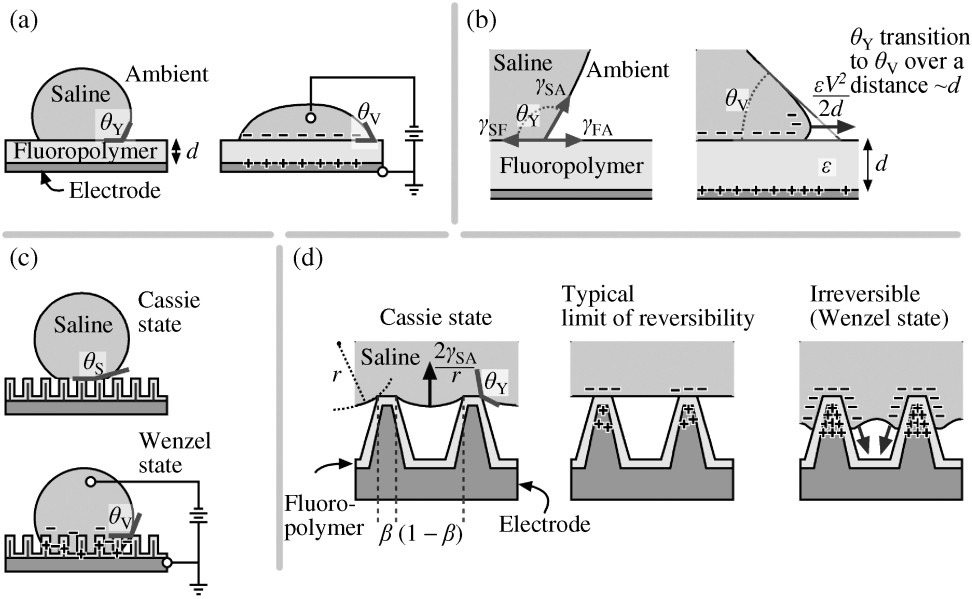


Figure 1. Wetting and electrowetting diagrams with: (a) macroscopic view of a planar hydrophobic surface, (b) microscopic view of the contact line for a planar hydrophobic surface, (c) macroscopic view of Cassie and Wenzel wetting states for a structured super-hydrophobic surface and (d) microscopic view of electrowetting on a structured super-hydrophobic surface. The above diagrams are qualitative representations. The diagrams are not representative of all possible approaches since many liquids, dielectric thicknesses, and structure morphologies are possible.

component in the horizontal direction. This results in a horizontal electromechanical force per unit length (mN/m) that is directed from the saline phase toward the ambient phase. As shown qualitatively in Fig. 1b, this force per unit length [11] results in deformation of the droplet and a saline meniscus that *projects* to a new reduced contact angle θ_V. However, as also shown in Fig. 1b, the microscopic or 'local' contact angle is always Young's angle θ_Y [12]. Although this short explanation does not contain the full spirit and details of the electromechanical electrowetting theory [11], Young's equation and a simplified electrowetting equation can be provided as:

$$\gamma_{SF} = \gamma_{FA} - \gamma_{SA}\cos\theta_Y, \tag{1a}$$

$$\cos\theta_V = \cos\theta_Y + \frac{1}{2}\cdot\frac{\varepsilon\cdot V^2}{\gamma_{SA}\cdot d}, \tag{1b}$$

where d is the dielectric thickness, ε the dielectric permittivity, ε/d the dielectric capacitance per unit area (F/m^2) of the dielectric, and V is the applied DC voltage or AC RMS voltage. The importance of the local contact angle always being Young's can be further appreciated after reading the following discussion.

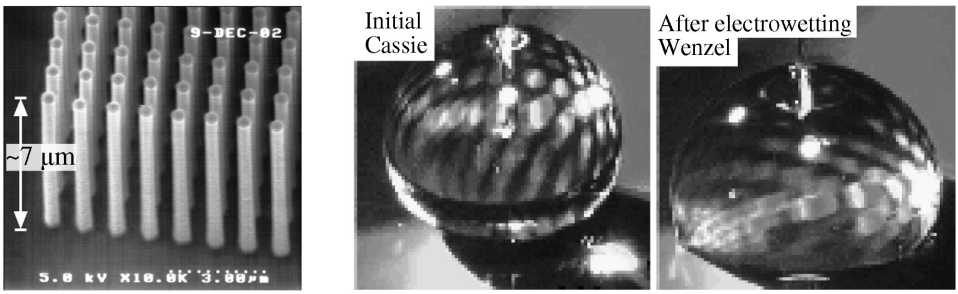


Figure 2. Photographs of: (a) Si nanoposts and (b) saline droplets in the Cassie and electrowetted Wenzel states. Images are reprinted with permission from [13], copyright 2004 American Chemical Society.

Qualitative diagrams of electrowetting on structured surfaces are shown in Fig. 1c and 1d. As pictured, the surfaces have a superhydrophobic water contact angle (>150°), but the discussion here also applies to structured electrowetting surfaces that are not superhydrophobic. In the diagram the droplet rests upon hydrophobic posts and the air that fills the space between the posts. This is often referred to as the Cassie, or Cassie–Baxter state, and is practically achieved if the side-wall slope of the posts and θ_Y provide a saline meniscus which is convex between the hydrophobic posts. A photograph from [13] of a droplet in the Cassie state on Si nano-posts, and an SEM image of the posts is shown in Fig. 2. As labeled in Fig. 1d, this convex meniscus has a corresponding Young–Laplace pressure ($\Delta p \propto 2\gamma_{SA}/r$) that prevents liquid from wetting into the space between posts. This requires that the post spacing be close enough (typically μm's) to counteract gravitational and other pressures that might cause wetting into the space between the posts. However if superhydrophobicity is to be achieved, the fraction of the saline surface that contacts the low surface energy posts (β) should be much less than the fractional area of the saline contacting the air ($1-\beta$). This reduced contact area for the saline leads to both an altered initial contact angle at zero voltage (θ_S) and also reduces the electrical capacitance between the saline and the electrode. As a first approximation such an electrowetting system on a structured surface can therefore be predicted by the Cassie–Baxter [14] equation (2a) and a modified electrowetting equation (2b) provided by Torkelli [15]:

$$\cos\theta_S = \beta(1+\cos\theta_Y) - 1, \tag{2a}$$

$$\cos\theta_V = \cos\theta_S + \frac{1}{2}\cdot\frac{\beta\cdot\varepsilon\cdot V^2}{\gamma_{SA}\cdot d}. \tag{2b}$$

Up until this point we have only considered wetting for the Cassie state and no electrowetting into space between the posts. So long as electrowetting is performed in the Cassie state it is reversible on superhydrophobic surfaces. Irreversibility oc-

curs as the electromechanical electrowetting force exceeds the combined effects of Young–Laplace pressure and contact angle hysteresis, thus resulting in wetting of the saline into the spaces between the posts. With the saline having advanced into the space between the posts two scenarios exist, one largely hypothetical, one practical. The largely hypothetical case is as follows. If the advancement of the saline meniscus between the posts does not reach the bottom surface, and if the contact angle hysteresis is small, removing the voltage could lead to reversibility of wetting as the Young–Laplace pressure drives the liquid from between the posts. For substrates with very small structures (∼μm) this situation is most often hypothetical since the electrowetting occurs in milliseconds or less and the saline quickly reaches the lower substrate surface. Therefore, the practical (often observed) scenario is that once sufficient voltage is applied the liquid quickly reaches the lower surface between the posts and a stable Wenzel state is achieved. Once the Wenzel state is achieved, for most materials and structure geometries the system has found a new energy minimum and wetting is irreversible. A photograph of a droplet that has achieved the Wenzel state is shown at right in Fig. 2b [13]. The earlier discussion that Young's angle is always preserved at the contact line should now be revisited. The wetting into the structured surface should not be directly linked to a traditional capillary wetting event due to the Young–Laplace pressure of a *concave* saline meniscus. This is because Young's angle always manifests itself over a distance comparable to the dielectric thickness [12]. Therefore, for structures where the dielectric thickness is comparable to the spacing between posts, this convex to concave transition for wetting into the dielectric may not occur. However, according to electrowetting/dielectrophoresis and Pellat experiments of Jones [16], independent of the saline meniscus curvature, the electromechanical force will still drive saline into a capillary. Therefore, as concluded by Jones [16] and Mugele and Buehrle [12] liquid movement in electrowetting structures should not be directly attributed to change in microscopic contact angle.

3. Fabrication of Structured Electrowetting Surfaces

Real-world structured surfaces for superhydrophobic electrowetting range from geometrically uniform like those in Figs 1d and 2a, to randomly oriented fiber-like structures. Most demonstrated works include a composite dielectric approach. In this composite approach the structured electrode is first insulated with a conventional dielectric such as a metal or semiconductor oxide. The composite dielectric is then completed with a plasma deposited fluorocarbon or solution deposited fluoropolymer in order to provide adequate hydrophobicity for a stable Cassie state. A brief review of techniques to create superhydrophobic electrowetting surfaces is provided below. The demonstrated structures vary substantially in geometry and materials, however, electrowetting results are somewhat similar across all platforms.

Early Work — Reported in the thesis of Torkelli [15] are investigations of numerous superhydrophobic electrowetting structures, including precursors to all the post-like and nanobrick features found in this review. Torkelli also demonstrated nano and microstructured surfaces such as posts, but with additional micro-scale surface roughness on the posts to further increase the hydrophobicity. Conventional wetting was characterized for each structure. However, electrowetting characterization was reported only for a few structures and there are insufficient data for comparative analysis in this review.

3.1. Silicon Nanoposts

The structures pictured in Fig. 2a are Si nanoposts [13]. The Si nanoposts were etched into a Si substrate *via* deep reactive ion etching. The Si posts had a very high aspect ratio of 20:1, with a 350 nm diameter and 7 μm height. Posts were tested with center-to-center pitches ranging from ∼1 μm to ∼4 μm. In order to form a dielectric, the posts were first thermally oxidized with 50 nm of SiO_2. Thermally grown SiO_2 forms an exemplary dielectric since it is conformal, pin-hole free, and has a high breakdown field (>4 MV/cm). Next a 20 nm thick fluorocarbon layer was deposited *via* plasma-assisted chemical vapor deposition. As shown in Table 1, this structured surface exhibited a local Young's angle of $\theta_Y \sim 90°$ for a water:methanol mixture and a macroscopically observed structured contact angle of $\theta_S \sim 160°$. For this work, the electrowetting data were acquired using not water, but using a molten salt with $\gamma_{SA} \sim 62$ mN/m. It is worth noting that on these Si nanoposts electrowetting of low surface tension liquids such as cyclopentanol was also tested. The cyclopentanol formed an immobile droplet on the substrate, and with applied voltage resulted in very low contact angle and wetted most of the available substrate area.

3.2. Epoxy Microposts

Photolithography can also be utilized to create a superhydrophobic surface (Fig. 3a). An exemplary photoresist material for this purpose is SU-8 (MicroChem), an ultra-violet cured photo-epoxy. Because SU-8 has excellent transmission to ultraviolet light, it can be photolithographically processed in very thick films (even up to ∼1 mm). In creating a superhydrophobic electrowetting surface, SU-8 was patterned into micro-posts with dimensions of ∼7 μm diameter, ∼15 μm pitch, and ∼6.5 μm height [17, 18]. A metal film beneath the SU-8 provided the lower electrode, and a solution coating of DuPont Teflon AF provided a hydrophobic surface. The Teflon AF was spin coated resulting in a parallel network of ridges between posts (Fig. 3a). As detailed in Table 1, this structured surface exhibited a local Young's angle of $\theta_Y \sim 115°$ and a macroscopically observed contact angle of $\theta_S \sim 150°$. Because the electrode lies fully beneath the surface structures, it should be noted that this approach has reduced saline/electrode capacitance compared to the structure shown in the diagram of Fig. 1d. However, this buried electrode struc-

Table 1.
Summary of works dealing with electrowetting of highly polar liquids (saline or molten salts) on structured and superhydrophobic surfaces

Structure	Young's angle if planar (θ_Y)	Structured surface angle (θ_S)	Minimum reversible electrowetted angle (θ_V)	Minimum electrowetted angle (θ_V)/ voltage	Extrinsic dewet method	Author(s), year, (Ref.)
Numerous structures	–	~150°–165°	–	~140°/250 V	–	Torkelli, 2003, [15]
1 μm Pitch Si nanoposts	~90°	~160°	–	~95°/60 V	–	Krupenkin *et al.*, 2004, [13]
4 μm Pitch Si nanoposts	~90°	~160°	–	~100°/50 V	–	Krupenkin *et al.*, 2004, [13]
Si nanoposts and nanobricks with heater	–	~150°	–	–	10's ms boiling	Krupenkin *et al.*, 2007, [24]
Epoxy microposts	~115°	~150°	–	~95°/130 V	–	Herbetson *et al.*, 2006, [17]
Carbon nanofibers	~115°	~155°	~150°	~110°/40 V	Added oil	Dhindsa *et al.*, 2006, [19]
Carbon nanofibers (in oil ambient)	~160°	~160°	~120°	~120°/68 V	In oil ambient	Dhindsa *et al.*, 2006, [19]
Si nanowires	–	~160°	~140°	–		Verplanck *et al.*, 2007, [21]
Si nanowires (in oil ambient)	–	~160°	~110°	~110°/150 V	In oil ambient	Verplanck *et al.*, 2007, [21]
Carbon nanotubes (with dielectric)	~70°	~110°	–	~90°/80 V	–	Wang *et al.*, 2007, [22]
Carbon nanotubes (no dielectric)	~90°	~155°	–	~50°/8 V	–	Zhu *et al.*, 2006, [23]

ture can prove experimentally useful since the Wenzel roughness can be extracted from the contact angle change *vs.* voltage data [17].

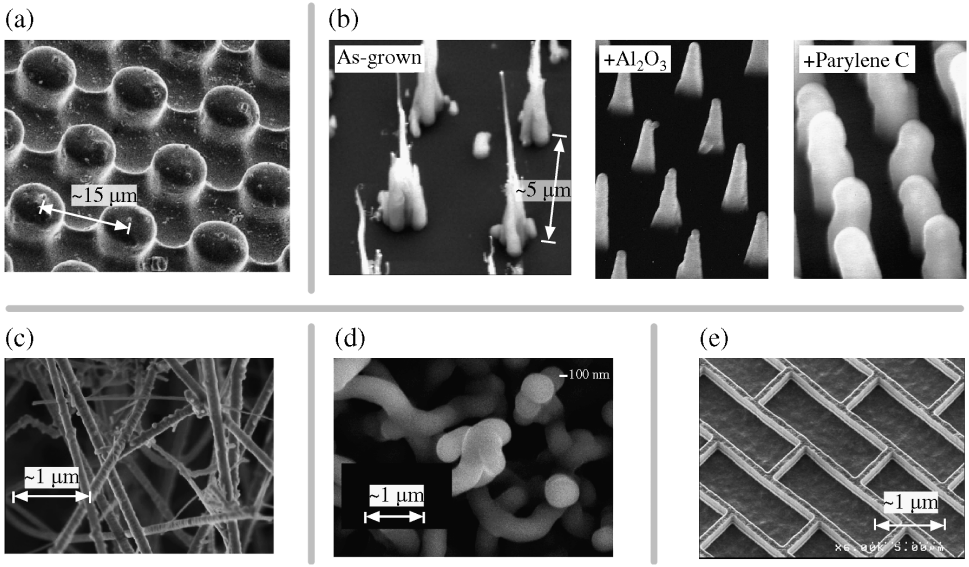


Figure 3. Additional photographs of superhydrophobic electrowetting surfaces including: (a) epoxy microposts [17], (b) carbon nanofiber scaffold with aluminum oxide or Parylene C dielectric coating [19], (c) silicon nanowires with fluorocarbon coating [21], (d) carbon nanotubes with Parylene C coating [22] and (e) silicon nanobricks with oxide and fluorocarbon coating [15, 24]. All images are reprinted with permissions: (a) 2005 Elsevier B.V., (b) 2006 American Chemical Society and (c, d, e) 2007 American Chemical Society.

3.3. Carbon Nanofibers

As shown in Fig. 3b, vertical carbon nanofibers are not as geometrically regular as Si nanoposts or epoxy microposts, but are equally capable of superhydrophobic electrowetting behavior [19]. These electrically conductive carbon nanofibers were grown *via* a chemical vapor deposition process. Regular $\sim 5 \times 5$ μm arrays of nanofibers were created by patterning a growth catalyst on a Si substrate [20]. The nanofibers are >10 μm in height and terminate with <50 nm diameter tips. Also as shown in Fig. 3b, two highly-conformal dielectric coating techniques were demonstrated. In one approach, a ~200 nm thick layer of Al_2O_3 was deposited *via* atomic layer deposition. In another approach, ~1.1 μm of organic Parylene C was deposited. Generally, organic dielectrics need be thicker than inorganic dielectrics due to a lower electrical breakdown field for the former. Both sets of structures were completed by solution coating with ~350 nm of fluoropolymer. Not only were the completed structures more geometrically irregular than the Si nanoposts or epoxy microposts, but the structures also differed by exhibiting hemispherical tips. As shown in Table 1, this carbon nanofiber surface exhibited a local Young's angle of $\theta_Y \sim 115°$ and a macroscopically observed contact angle of $\theta_S \sim 155°$.

3.4. Silicon Nanowires

A second form of Si-based structures has been recently demonstrated in the form of silicon nanowires [21]. The nanowires differ from nanoposts in that they are not vertically aligned, and as seen in Fig. 3c nanowires exhibit even more geometrical irregularity than carbon nanofiber arrays. The nanowires were grown using a chemical vapor deposition process in combination with catalyst particles that were randomly patterned across the substrate. The Si nanowires were insulated with 350 nm of silicon oxide and made hydrophobic through a fluorocarbon coating. As detailed in Table 1, the structured nanowire surface exhibited a macroscopically observed contact angle of $\theta_S \sim 160°$.

3.5. Carbon Nanotubes

A second form of carbon-based structures has been recently demonstrated in the form of multi-wall carbon nanotubes. As detailed in Table 1, electrowetting results have been shown with a dielectric coating [22] or without a dielectric coating [23]. Like nanowires and nanofibers, the nanotubes were grown *via* chemical vapor deposition in the presence of a catalyst particle. For the dielectric coated structures, Parlyene C was coated at ∼200 nm thickness and the completed structures are shown in Fig. 3d. As detailed in Table 1, with $\theta_Y \sim 70°$ these structures did not achieve superhydrophobicity. In fact θ_S only reached ∼110°, and one might conclude that capillary wetting into the structures likely occurred in some locations even without application of voltage. However, for the report of electrowetting on carbon nanotubes with no dielectric, an initial superhydrophobic state of $\theta_S \sim 155°$ was achieved [23]. Without the dielectric, the capacitance in equation (2b) is determined by the electrical double layer capacitance and the required electrowetting voltage is substantially lowered. Also, without a dielectric the saline experiences electrolysis, and the wetting is always irreversible. As a result, nearly all present-day electrowetting research utilizes a physical dielectric between the saline and the electrode.

3.6. Other Structures

As shown in Fig. 3e, the process used for creating Si nanoposts has also been used to create nanobricks with $\theta_S \sim 160°$ [24]. These structures are similar to those first reported by Torkelli [15].

4. Electrowetting Results on Superhydrophobic Surfaces

The largest single data set for electrowetting on a superhydrophobic surface can be found in Dhindsa *et al.*'s work on carbon nanofibers [19]. Here, electrowetting results *vs.* voltage for two different dielectric materials and thicknesses were measured *via* both contact angle and electrical capacitance. This data set is therefore the example data set chosen for this review. For a uniformly structured surface,

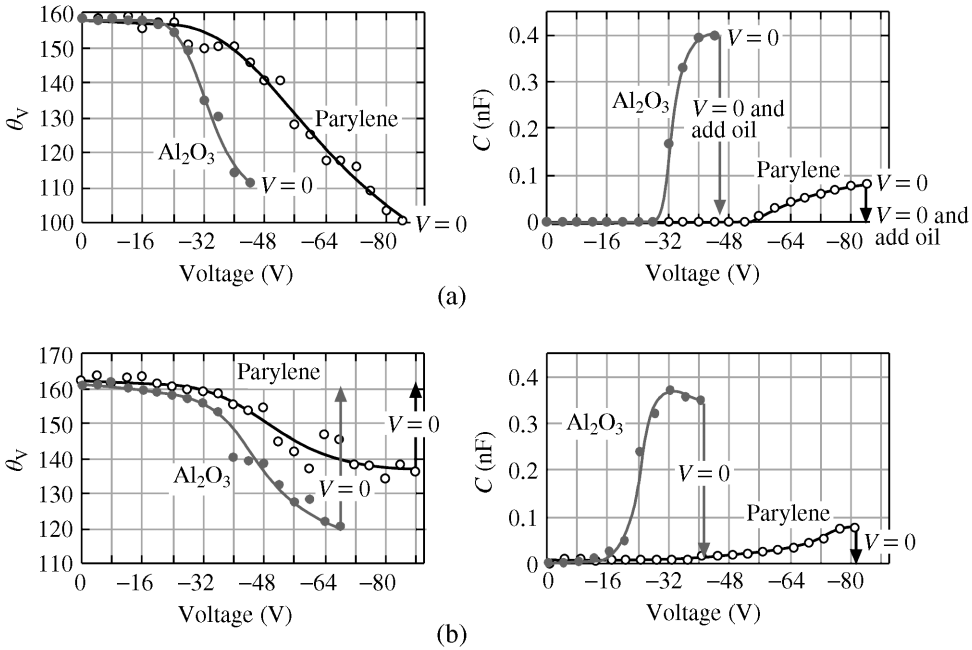


Figure 4. Plots of contact angle and capacitance for carbon nanofiber system (a) a saline droplet in an air ambient and (b) a saline droplet in a dodecane (oil) ambient. At the end of all experiments the voltage was removed and the final contact angle is labeled. Images are reprinted with permission from [19], copyright 2006 American Chemical Society.

such as one comprised of regular flat-top pillars like those of Fig. 1d, as one increased the applied voltage one would expect a nearly instantaneous transition from a superhydrophobic Cassie state to the Wenzel state. This rapid transition is apparent in the contact angle *vs.* voltage curves reported by Krupenkin *et al.* in [13] for the nanoposts shown in Fig. 2. However, as shown in Fig. 4a, the electrowetting on carbon nanofibers exhibits a more gradual response. This is because the geometrical variations between individual nanofibers broaden the contact angle *vs.* voltage response. That is to say, on a local scale the transition from the Cassie to Wenzel state occurs at different voltages. These voltages depend on the geometry of local groups of nanofibers (converging, diverging, rough, etc.). Also notable in the plots of Fig. 4a, the Al_2O_3-coated carbon nanofibers achieve electrowetting at 10's of volts less than the Parylene-coated samples. This is because the samples with Al_2O_3/fluoropolymer coating have higher capacitance and a less vertical sidewall slope of 80–85°. The effect of higher capacitance is readily appreciated with inspection of equations (1b) and (2b). The electromechanical force that drives electrowetting is due to charge accumulation near the contact line. A larger electrical capacitance allows charge accumulation to occur at lower voltage ($Q = CV$). The effect of sidewall slope is related to the effect of Young–Laplace pressure described

for Fig. 1. Simply, if the saline meniscus faces toward converging sidewall geometry, it will have a larger radius of curvature and a reduced Young–Laplace pressure. In fact, one must not increase the sidewall slope too much, since a Young's angle of 115° and a sidewall slope of 65° would result in a flat meniscus which is already at the threshold for capillary wetting. For the carbon nanofiber experiments, the maximum electrowetted contact angle change was observed to be $\theta_S \sim 160°$ to $\theta_V \sim 100°$ for the Parylene sample. In both the Al_2O_3 and Parylene data sets, the data were taken to the point where the contact angle reduction was observed to saturate. The electrowetting was only slightly reversible over a range of 160–150°. The role of materials and structure geometry on reversibility is discussed in a later section. It is also important to note that the total dielectric thickness for the Parylene/fluoropolymer coated nanofibers was ~1.4 μm. This is comparable to the remaining spacing of ~2 μm between the nanofibers on a 5 × 5 μm pitch. Therefore, even during electrowetting Young's angle will project over a significant portion of the space between the fibers. Thus, this set of electrowetting data provides an experimental example of why the wetting between the fibers should *not* be directly linked to contact angle change, and should be attributed to electromechanical forces. Another distinct example could be found upon closer examination of Herbertson *et al.*'s work on epoxy microposts [17]. The microposts are electrical insulators formed on a conductive substrate, the electric field has a large vertical component, and the entire liquid meniscus between the microposts should experience a substantial downward *electromechanical* force that causes the Cassie to Wenzel transition (i.e. not directly linked to sidewall contact angle).

Also provided in Fig. 4a is a plot of electrical capacitance *vs.* applied voltage. The electrical capacitance is measured between the saline and the nanofiber electrodes. This is a useful experimental technique as it provides direct measurement of the droplet progress from the Cassie state (minimum capacitance) to the Wenzel wetting state (maximum capacitance). Like the measurements of contact angle *vs.* voltage, the capacitance measurements for the Al_2O_3 coated sample exhibited a sharper and lower voltage electrowetting response. Saturation of the capacitance increase indicates that the Wenzel state has been reached at nearly all spaces beneath the saline droplet. It is important to note that the onset of a macroscopically observed saturation in contact angle change on a superhydrophobic electrowetting surface indicates successful transition from the Cassie to Wenzel state, but it does not necessarily correlate with the onset of contact angle saturation at the microscopic scale. For most works reviewed here, the dielectric layers are very thin. Therefore, for most works, if microscale electrowetting saturation does occur, it is therefore likely due to charge injection into the dielectric coating [25] or current flow after electrical breakdown of the dielectric. Discussion on the role of oil in the plots of Fig. 4 is reserved for the next section on wetting reversibility.

These carbon nanofiber experiments provide a good example of electrowetting on a superhydrophobic surface. This is not because the acquired data are of a higher

quality or are unique in any important manner. Rather, it is because currently all electrowetting experiments on superhydrophobic surfaces have exhibited similar results. Considering the widely varied geometries and materials used to create the surfaces reviewed here, this consistency in electrowetting results may be surprising. Inspecting the results of Table 1 the following similarities can be concluded. First, most experiments show a contact angle reduction from $\theta_S \sim 160°$ to $\theta_V \sim 100°$. Secondly, if achieved at all, reversibility is limited to a small range of $\sim 20°$. Therefore, the collective body of work suggests that future investigations should involve significantly different geometrical structures and materials if a wider range of electrowetting contact angle change is to be achieved. It is also worth noting that most structures had high capacitance dielectric coatings. High capacitance leads to a more rapid onset of electrowetting. However, in the superhydrophobic electrowetting works reviewed here, the dominant factor in the steepness of the transition from the Cassie to the Wenzel state was not capacitance, but the geometrical regularity of the structures.

5. Techniques for Reversible Electrowetting on Superhydrophobic Surfaces

From an applications standpoint, it is important to improve the reversibility of electrowetting on superhydrophobic surfaces. Few applications have been suggested if the wetting is irreversible, one of them being a reserve battery structure demonstrated by Lifton *et al.* [26]. For applications such as lab-on-chip [5, 6], improved reversibility could allow droplet movement of physiological fluids on a superhydrophobic surface. Torkelli was able to demonstrate lateral electrowetting droplet movement on a superhydrophobic surface [15]. One benefit of the superhydrophobicity would be improved resistance to surface fouling, possibly even allowing the movement of large particulates inside the liquid (i.e. a self-cleaning surface). Extrinsic techniques for reversible electrowetting on a superhydrophobic surface have been reported. These techniques are reviewed below, and are classified as extrinsic because they require materials or device designs that are beyond the basic electrowetting construction of saline/dielectric/electrode.

As shown in the plots of Fig. 4, Dhindsa *et al.* reported that at no applied voltage the addition of dodecane oil to a droplet in the Wenzel state caused dewetting of the droplet to the Cassie state [19]. In the plots of Fig. 4, this dewetting event is labeled as "$V = 0$ and add oil" for an air ambient, or "$V = 0$" for an oil ambient. It should be noted that when the air ambient is replaced by the oil the term superhydrophobic is taken out of its original context of an air ambient. To elaborate further, a saline droplet in an oil ambient easily achieves a Young's angle of $\theta_Y > 160°$ even on a planar Teflon substrate, but this should *not* be classified as superhydrophobic surface in light of the traditional meaning of the term. The reversibility of the carbon nanofiber system plotted in Fig. 4 is achieved in one of two ways: (a) electrowetting in an air ambient to the point of an irreversible Cassie to

Wenzel transition, followed by adding enough oil to cause dewetting as oil replaces the water in the space between the nanofibers; (b) performing the electrowetting experiment in an oil bath. The reversibility can be partially explained as follows, and may shed some light on new structures that might be designed in the future. Adding dodecane oil to the system somewhat reduces the saline/ambient interfacial tension from ∼73 mN/m to ∼50 mN/m. Adding oil to the system also changes Young's angle on the fluoropolymer from $\theta_Y \sim 115°$ to $\theta_Y > 160°$. This increased Young's angle has an important effect between the nanofibers since the convexity of the saline meniscus in the presence of oil is therefore much larger. This increases Young–Laplace pressure ($\Delta p \propto 2\gamma_{SA}/r$) and the ability for the saline to dewet from the Wenzel state. Furthermore, it is well known that the oil decreases contact angle hysteresis substantially (∼1°) which should further facilitate the dewetting process. This brings up a question, for the data presented by Dhindsa *et al.* where does the oil come from? First, it is expected that some small amount of oil remains trapped between the nanofibers. When the voltage is removed, the remaining influx of oil must flow horizontally through the nanofibers, and the saline droplet dewets as the oil advances and contact line recedes.

Krupenkin *et al.* have demonstrated rapid substrate heating [24] as a means of enabling reversible electrowetting of the Si nanoposts and nanobricks shown in Fig. 3. This approach embeds a micro-heating element immediately beneath the structured surface. For a droplet that has been electrowetted to the Wenzel state, a current spike for 10's of ms duration is run through the heating element and during that same time frame the saline experiences boiling at its interface with the substrate. The effect is extremely rapid, produces a water vapor blanket beneath the saline droplet and the droplet is actually launched slightly above the substrate. The droplet then comes to rest on the substrate in the Cassie state, and the wetting/dewetting cycle can be repeated many times. From an applications standpoint, this technique could prove useful since it is performed in an air ambient.

To reiterate, the above-described techniques provide extrinsic means of creating reversibility. Other techniques listed in Table 1 have shown that intrinsic reversibility is limited to ∼10–20°. As diagrammed and described for Fig. 1, the limit of intrinsic reversibility for the structures reviewed here occurs at the threshold for the transition from the Cassie to Wenzel state.

6. Conclusions and Speculation on Future Directions

A wide range of superhydrophobic surfaces have now been reported and are reviewed here. Most experiments show a contact angle reduction from $\theta_S \sim 160°$ to $\theta_V \sim 100°$ and a very limited intrinsic reversibility of ∼10–20°. Simply achieving the irreversible Wenzel state could be of use for applications such as infusing polar epoxies into fiber reinforcements for the creation of composite materials. If improved reversibility is desired, then there are likely numerous structures that have

yet to be investigated. Structures for improved reversibility might be inspired by recent work on creating superhydrophobic surfaces on materials that exhibit a hydrophilic Young's angle [27]. In this work, posts are replaced by structures that have the geometry of inverted pyramids or cones (i.e. flat at the top, tapering to the smallest diameter near the substrate). From the perspective of the droplet (i.e. downward) the capillary geometry is now *diverging*. This increases the Young–Laplace pressure that electrowetting must overcome before the onset of the Wenzel state can occur. However, assuming such a structure is created, a simple calculation with equation (2a) reveals that reversibility is still limited. Assuming a saline/structure contact area fraction of $\beta = 0.3$, and Young's angle of $\theta_Y = 125°$, equation (2a) predicts a structured contact angle that is nearly superhydrophobic with $\theta_S \sim 148°$. Next, assume the inverted pyramids have a diverging sidewall slope of 50° which therefore allows electrowetting contact angle modulation down to 40° without having to leave the Cassie state (i.e. no liquid penetration into the capillaries between the pyramids). The important point to be made is that theoretically the resulting macroscopically observed droplet contact angle still only reduces to $\theta_V \sim 118°$. Thus, the maximum reversibility range that one would expect is only ~30°. Clearly significantly different approaches are needed. Recent innovations that are highly distinct from the work reviewed here include liquid marbles [28] demonstrated by McHale *et al.* In this approach a droplet picks up a surrounding sheath of hydrophobic particles. Other ideas may include switching from post or fiber geometries to very small capillaries that essentially trap the air beneath the saline. The challenge here would be fabrication and achieving a small value for β. To expedite progress, researchers might first turn to modeling techniques that have already been utilized to model electrowetting on superhydrophobic surfaces [29]. This modeling work based on energy-minimization provides further theoretical explanation of the results achieved by Krupenkin *et al.* [13] and Herbertson *et al.* [17]. An improved understanding is provided for the energy barrier between the Cassie and Wenzel states, and similar work in the future might be used to predict the geometries and materials needed for fully reversible electrowetting on superhydrophobic substrates. Future work should also involve moving from the semiconductor manufacturing techniques used for all works reviewed here to those used for textiles and large area coatings. Recent reports of non-woven electrowetting textiles with a roughness enhanced contact angle of $\theta_S \sim 130°$ provide evidence that simpler fabrication techniques are achievable [30]. Even without present achievement of real-world applications, investigation of electrowetting on structured surfaces has enhanced understanding of wetting on and into micro and nanostructured surfaces.

Acknowledgements

The authors wish to acknowledge that their own research in electrowetting of carbon nanofibers is supported by collaborators at the University of Tennessee and

Oak Ridge National Laboratory (P. Rack and J. D. Fowlkes), and is financially supported by the National Science Foundation, Division of Chemical, Bioengineering, Environmental and Transport Systems Award #0729250.

References

1. F. Mugele and J.-C. Baret, *J. Phys.: Condens. Matter* **17**, 705 (2005).
2. Electrowetting related patents and publications have grown at an annual rate of ∼70% since 2001. Source: data compiled by J. Feenstra, LiquaVista Inc., Eindhoven (2007).
3. B. Berge and J. Peseux, *Euro. Phys. J. E., Soft Matter* **3**, 159 (2000).
4. More information on electrowetting lens commercialization can be found at www.varioptic.com
5. M. G. Pollack, R. B. Fair and A. D. Shenderov, *Appl. Phys. Lett.* **77**, 1725 (2000).
6. More information on electrowetting lab-on-chip commercialization can be found at www.liquid-logic.com
7. R. A. Hayes and B. J. Feenstra, *Nature* **425**, 383 (2003).
8. More information on electrowetting display commercialization can be found at www.liquavista.com
9. B. Berge, *C. R. Acad. Sci. Paris III* **317**, 157 (1993).
10. W. J. J. Welters and L. G. Fokkink, *Langmuir* **14**, 1535 (1998).
11. T. B. Jones, J. D. Fowler, Y. S. Chang and C. J. Kim, *Langmuir* **19**, 7646 (2003).
12. F. Mugele and J. Buehrle, *J. Phys.: Condens. Matter* **19**, 375112 (2007).
13. T. N. Krupenkin, J. A. Taylor, T. M. Schneider and S. Yang, *Langmuir* **20**, 3824 (2004).
14. A. B. D. Cassie and S. Baxter, *Trans. Faraday Soc.* **3**, 16 (1944).
15. A. Torkelli, *Droplet microfluidics on a planar surface*. PhD Thesis, Department of Electrical Engineering, Helsinki University of Technology, Espoo, Finland (2003).
16. T. B. Jones, *J. Micromech. Microeng.* **15**, 1184 (2005).
17. D. L. Herbertson, C. L. Evans, N. J. Shirtcliffe, G. McHale and M. I. Newton, *Sensors Actuators A* **130–131**, 189 (2006).
18. N. J. Shirtcliffe, S. Aqil, C. Evans, G. McHale, M. I. Newton, C. C. Perry and P. Roach, *J. Micromech. Microeng.* **14**, 1384 (2004).
19. M. Dhindsa, N. Smith, J. Heikenfeld, J. Fowlkes, P. D. Rack, M. J. Doktycz, A. V. Melechko and M. L. Simpson, *Langmuir* **22**, 9030 (2006).
20. T. E. McKnight, C. Peeraphatdit, S. W. Jones, J. D. Fowlkes, B. L. Fletcher, K. L. Klein, A. V. Melechko, M. J. Doktycz and M. L. Simpson, *Chem. Mater.* **18**, 3203 (2006).
21. N. Verplanck, E. Galopin, J.-C. Camart, V. Thomy, Y. Coffinier and R. Boukherroub, *Nano Lett.* **7**, 813 (2007).
22. Z. Wang, Y. Ou, T. M. Lu and N. Koratkar, *J. Phys. Chem. B* **111**, 4296 (2007).
23. L. Zhu, J. Xu, Y. Xiu, Y. Sun, D. W. Hess and C.-P. Wong, *J. Phys. Chem. B* **110**, 15945 (2006).
24. T. N. Krupenkin, J. A. Taylor, E. N. Wang, P. Kolodner, M. Hodes and T. R. Salamon, *Langmuir* **23**, 9128 (2007).
25. H. J. J. Verheijen and M. W. J. Prins, *Langmuir* **15**, 6616 (1999).
26. V. A. Lifton, S. Simon and R. E. Frahm, *Bell Labs Technical J.* **10**, 81 (2005).
27. L. Cao, H.-H. Hu and D. Gao, *Langmuir* **23**, 4310 (2007).
28. G. McHale, D. L. Herbertson, S. J. Elliott, N. J. Shirtcliffe and M. I. Newton, *Langmuir* **23**, 918 (2007).

29. V. Bahadur and S. V. Garimella, *Langmuir* **23**, 4918 (2007).
30. K. Bhat, J. Heikenfeld, M. Agarwal, Y. Lvov and K. Varahramyan, *Appl. Phys. Lett.* **91**, 024103 (2007).